geosciences

MDPI

Article

Assessment of Five Monazite Reference Materials for U-Th/Pb Dating Using Laser-Ablation ICP-MS

Marianne Richter [1,*], Yona Nebel-Jacobsen [1], Oliver Nebel [1], Thomas Zack [2], Regina Mertz-Kraus [3], Massimo Raveggi [1] and Delia Rösel [2,4]

1 Isotopia Laboratory, School of Earth, Atmosphere and Environment, Monash University, 9 Rainforest Walk, 3800 Clayton, VIC, Australia; Yona.Nebel-Jacobsen@monash.edu (Y.N.-J); Oliver.Nebel@monash.edu (O.N.); Massimo.Raveggi@monash.edu (M.R.)

2 Department of Earth Sciences, University of Gothenburg, Box 460, SE-405 30 Göteborg, Sweden; thomas.zack@gu.se (T.Z.); delia.rosel@gu.se (D.R.)

3 Institut für Geowissenschaften, Johannes Gutenberg-Universität Mainz, J.-J.-Becher-Weg 21, D-55128 Mainz, Germany; mertzre@uni-mainz.de

4 Institut für Geologie, Technische Universität Bergakademie Freiberg, Bernhard-von-Cotta-Straße 2, D-09599 Freiberg, Germany; delia.roesel@geo.tu-freiberg.de

* Correspondence: Marianne.Richter@monash.edu

Received: 24 May 2019; Accepted: 3 September 2019; Published: 6 September 2019

Abstract: Monazite is a common accessory phosphate mineral that occurs under a wide range of pressure and temperature conditions in sedimentary, metamorphic and igneous rocks. Monazite contains high amounts of Th and U, rendering single monazite grains suitable for in-situ U-Th/Pb dating using laser ablation inductively-coupled mass spectrometry (LA-ICP-MS). Two key aspects of monazite dating that are critical for accurate age data with maximum precision are (i) optimized instrumental conditions to minimize analytical scatter and (ii) a well characterized reference material to ensure the accuracy of the obtained aged. Here, we analyzed five monazite reference materials (USGS 44069, 94-222, MAdel, Moacir and Thompson Mine Monazite) for their U-Th/Pb ages using LA-ICP-MS technique and applied a variety of laser spot diameters and repetition rates to find the best operational conditions to achieve accurate age data while maintaining maximum precision. We find that a spot diameter of 10 µm and a repetition rate of 10 Hz yield the most precise ages with a deviation of ±2.0% from their respective high-precision U/Pb literature age data. Ages were reproduced in three different LA-ICP-MS laboratories using these parameters. Each reference material was tested for its suitability as a matrix-matched age reference material. For this, a rotating, iterative approach was adopted in which one reference monazite was used as calibration reference material against all others, which were treated as unknowns. The results reveal that USGS 44069, 94-222, Thompson Mine Monazite and MAdel all agree with their respective calculated ages and ID-TIMS reference ages and thus are suggested as suitable calibration reference materials. Moacir, however, appears slightly older than previously suggested (up to 4%), thus, caution is advised here when using Moacir as reference material for U-Th/Pb LA-ICP-MS dating in the absence of further absolute age calibration.

Keywords: monazite; reference material; Moacir; USGS 44069; TMM; MAdel; 94-222; U-Th/Pb dating; LA-ICP-MS

1. Introduction

Monazite [(Ce, La, Nd, Th)PO_4] is an accessory mineral that can contain large amounts of U (up to 6 wt.% UO_2), Th (< 1 to 30 wt.% ThO_2, common 4–12 wt.%) and light-rare earth elements (LREE) [1–3]. In general, monazite incorporates only negligible amounts of Pb [4], resulting in high U-Th/Pb ratios.

Therefore, monazite is increasingly used for U-Th/Pb dating in a wide range of geodynamics processes, e.g., [3,5–9].

Monazite U-Th/Pb ages can be determined using isotope dilution thermal ionization mass spectrometry (ID-TIMS), secondary ion mass spectrometry (SIMS), electron microprobe analysis (EMPA) and laser ablation inductively coupled mass spectrometry (LA-ICP-MS) technique, with each method having their own advantages and disadvantages [10,11]. For instance, ID-TIMS analyses achieve an age resolution of < ±0.1% [12], but require the dissolution of whole grains, resulting in the loss of spatial resolution for a mineral that commonly exhibits strong chemical zonation. In contrast, SIMS, EMPA and LA-ICP-MS analyses are in-situ techniques, allowing specific chemical zones to be targeted within a single grain with excellent spatial resolution. However, the age resolution of all three analytical techniques is lower than for ID-TIMS and ranges between ±0.4% for SIMS, to circa ±2% for LA-ICP-MS [13]. In addition, significant matrix problems can be encountered when using SIMS and EMPA for monazite dating, e.g., [14,15]. The main advantage of LA-ICP-MS, compared to ID-TIMS, EMPA and SIMS, is its relatively fast and low-cost set up, combined with its availability in many geoscience departments.

Of paramount importance for all of the above-mentioned methods is a suitable reference material (RM). At present, a range of RMs are used in the geochronology community for U-Th/Pb monazite dating, for example, Manangoutry [16–18], USGS 44069 [19], Moacir (also known as Moacyr) [8,20,21], MAdel [22], Thompson Mine Monazite (TMM) [23], UNIL Mnz-1 [24,25], 94-222 [26], Diamantina [27], FC1 [18], Trebilock [28], Elk [29], or Iveland [29,30]. However, to date, there is no consensus on either standardization of data or the use and suitability of RMs to ensure accurate dating results with maximum precision.

In this study, three commonly used and two in-house monazite RMs were chosen to assess their suitability as RM for U-Th/Pb age dating for LA-ICP-MS analyses. The assessment was performed by determining an analytical protocol, using a variety of operational settings, which then was applied to three different LA-ICP-MS laboratories.

2. Monazite Reference Materials

The five monazite RMs used in this study are 94-222 [22], USGS 44069 [19], MAdel [22], Moacir [20,31], and TMM [23]. A brief overview of all used RMs is provided below.

2.1. USGS 44069

Monazite sample USGS 44069 originates from an amphibolite- to granulite-facies meta-sedimentary unit (Wissahickon Formation) from the Wilmington Complex, Delaware (DE, USA). The age of reference monazite USGS 44069 is related to the amphibolite- to granulite-facies metamorphic overprint that occurred contemporaneously with the emplacement of the Arden Plutonic Supersuite between 435 and 425 Ma [19].

Aleinikoff et al. (2006) obtained precise and concordant $^{206}Pb/^{238}U$ ID-TIMS age of 424.9 ± 0.8 Ma (2s) (Table 1) that is consistent with a $^{206}Pb/^{238}U$ SHRIMP age of 426.0 ± 6.0 Ma (2s) of the same study. [32] obtained a $^{208}Pb/^{232}Th$ weighted mean LA-ICP-MS age of 416.2 ± 2.7 Ma (2s; n = 24). The reason for the age difference between the $^{208}Pb/^{232}Th$ age of the LA-ICP-MS study [32] and the $^{206}Pb/^{238}U$ ID-TIMS age [19] remains unknown and demands a more detailed investigation.

Monazite USGS 44069 is widely used in various studies as a calibration RM, e.g., [5,15,29,30,33–38]. Despite the above noted discrepancy, reference monazite USGS 44069 is an excellent RM for U-Th/Pb dating of monazite, because of its reliable age reproducibility [32,38].

2.2. 94-222

Monazite 94-222 originates from a garnet-bearing leucosome of the Harts Range Metamorphic Complex in the Irindina Province, SE Arunta Inlier, Central Australia (NT, Australia) [39–41]. The age has previously been interpreted to define the time of high-grade metamorphism and deformation in the Eastern Arunta Inlier.

Apparent discrepancies in the literature regarding the U/Pb age of reference sample 94-222 occurred. [41] analyzed monazite grains of the leucosome, using ion microprobe (SHRIMP), and obtained a $^{206}Pb/^{238}U$ age of 467 ± 16 Ma (2s). Monazites from the same location were analyzed under the sample name 'Bruna-NW' by [42] and obtained a U/Pb (LA-ICP-MS) age of 447.4 ± 5.6 Ma (2s). Even though within uncertainty, the large difference of 20 Myrs prompted [22] to re-evaluate monazite grains from the previous studies by [41,42] using the LA-ICP-MS technique. The re-evaluation resulted in a $^{206}Pb/^{238}U$ weighted mean age of 449.7 ± 6.8 Ma (2s) for monazite grains from both studies (Table 1). This example highlights the necessity for a coherent standardization. Monazite 94-222 is used mainly as an in-house RM at the University of Adelaide and has been applied in several studies using the age of 450 Ma, e.g., [37,40,43–45].

2.3. MAdel

The reference monazite MAdel originates from a single crystal (approximately 2 × 1 cm) from Madagascar from an unknown location (personal communication, J. Payne, 2013). ID-TIMS analyses identified two characteristic age domains with a difference in mean calculated ages of ca. 3 Myrs. The dominant age is the younger one with a $^{207}Pb/^{235}U$ age of 511.0 ± 2.6 Ma (2s). The older domain is less abundant and yields a $^{207}Pb/^{235}U$ age of 513.9 ± 3.2 Ma [2s; 22]. Even though both ages overlap with each other, the systematic shift points to an apparent absolute age difference of both domains. The age difference of 3 Myrs would result in a systematic bias in U-Th/Pb dating by LA-ICP-MS but cannot be resolved because of a lower precision of the method (uncertainty >1%, that is >5 Myrs). The $^{206}Pb/^{238}U$ age of 514.8 ± 3.6 Ma [2s; 22] is within uncertainty of the $^{207}Pb/^{235}U$ age.

MAdel, similar to 94-222, is used mainly as in-house calibration RM at the University of Adelaide [8,22,43] or as quality control material throughout the analysis [37,38].

2.4. Moacir (or Moacyr)

Moacir originates from the Itambè pegmatite district, Brazil [46,47]. The exact location of Moacir remains unknown [48]. [20] obtained a concordant U/Pb ID-TIMS age of 474 ± 1 Ma. [16] used Moacir as calibration RM in their LA-ICP-MS study but obtained younger Th/Pb and U/Pb ages for two other ID-TIMS monazite RMs (Manangoutry and Madagascar monazite) with resultant deviation of 4% and 8%, from the ID-TIMS literature age, respectively. Subsequent re-calibration experiments by [31] yielded a $^{207}Pb/^{235}U$ ID-TIMS age of 504.3 ± 0.4 Ma (Table 1) of Moacir. Further re-calibration of the Moacir by [21] yielded a $^{206}Pb/^{238}U$ ID-TIMS age of 513.0 ± 1.0 Ma (2s) spanning an age range of now 8% for ID-TIMS analyses to the originally reported TIMS value of 474 Ma [20].

2.5. Thompson Mine Monazite (TMM)

The Thompson Mine Monazite (TMM) originates from the Thompson Nickel Belt of central Manitoba, Canada [49,50] and has a U/Pb ID-TIMS reference age of 1766 ± 0.6 Ma (2s) [23]. TMM is frequently used in various studies as calibration RM [8,19,23,51–54] and is by far the oldest of the available monazites.

Table 1. Summary of all five analyzed monazite reference samples. [a,b]: References for the characteristics, ThO_2 and UO_2: [1]: [41], [2]: [19], [3]: [29], [4]: [10], [5]: observation based on this study, [6]: [26], [7]: [20], [8]: [16], [9]: [8], [10]: [23].

Reference Sample	Characteristics [a]	ThO_2 [wt.%] [b]	UO_2 [wt.%] [b]	Age ± 2s Uncertainty [Ma]	Dating Method	Locality	Reference Age
94-222	golden in color [1]; inclusion free [1]; size ranges between 200–500 µm [1]; minor compositional heterogeneity between core and rim [1]	5.52–10.41 [6]	0.23–0.62 [6]	449.7 ± 3.0	LA-ICP-MS	Harts Range Metamorphic Complex (Central Australia)	[26] [42] [41]
USGS 44069	discoidal to subhedral grains [2]; pale yellow in color [2]; grain size ~100 µm [2]; most grains having no zonation [2,3] while others show chemical inhomogeneity [4,5]	2.00–5.00 [2]	0.30–1.00 [2]	424.9 ± 0.8 424.0 ± 6.0	TIMS SHRIMP	Wilmington Complex (Delaware, USA)	[19]
MAdel	yellowish brown in color [5]; grain size between 200 and 400 µm [5]; most grains have chemical zonation [5]; two age domains with an age difference of 4 Ma [6]	8.98 [6]	0.43 [6]	511.0 ± 2.6 513.9 ± 3.2	TIMS	Madagascar	[22]
Moacir	yellow-orange in color and non-metamict [7]; crystal size is between 200–400 µm [7]; chemically homogenous [8], free of inclusions [8]	6.92 [7]	0.13 [7]	504.3 ± 0.4	TIMS	Itambè Pegmatite District (Brazil)	[31]
TMM	yellow to orange in color [5]; size vary between 100 to 300 µm [5]; grains show chemical zoning (patchy, oscillatory) [5]	7.0–19.0 [9]	0.23 [10]	1766.0 ± 26.0 1766.0 ± 0.6	LA-ICP-MS TIMS	Thompson Mine (Manitoba, Canada)	[8] [23]

3. Methods

3.1. Sample Preparataion

Several grains of each reference monazite were handpicked and jointly mounted on a 1-inch epoxy resin disc. The samples were polished down to the center of the grain using 600, 220, 9, 3 and 1 µm polishing discs. To identify a potential chemical zoning pattern, all analyzed monazite grains, backscattered electron (BSE) images (Figure 1) were taken using an electron microprobe JEOL JXA 8900 RL at the Institut für Geowissenschaften, Johannes Gutenberg-Universität in Mainz. An accelerating voltage of 15 kV and a beam current of ~11 nA was applied.

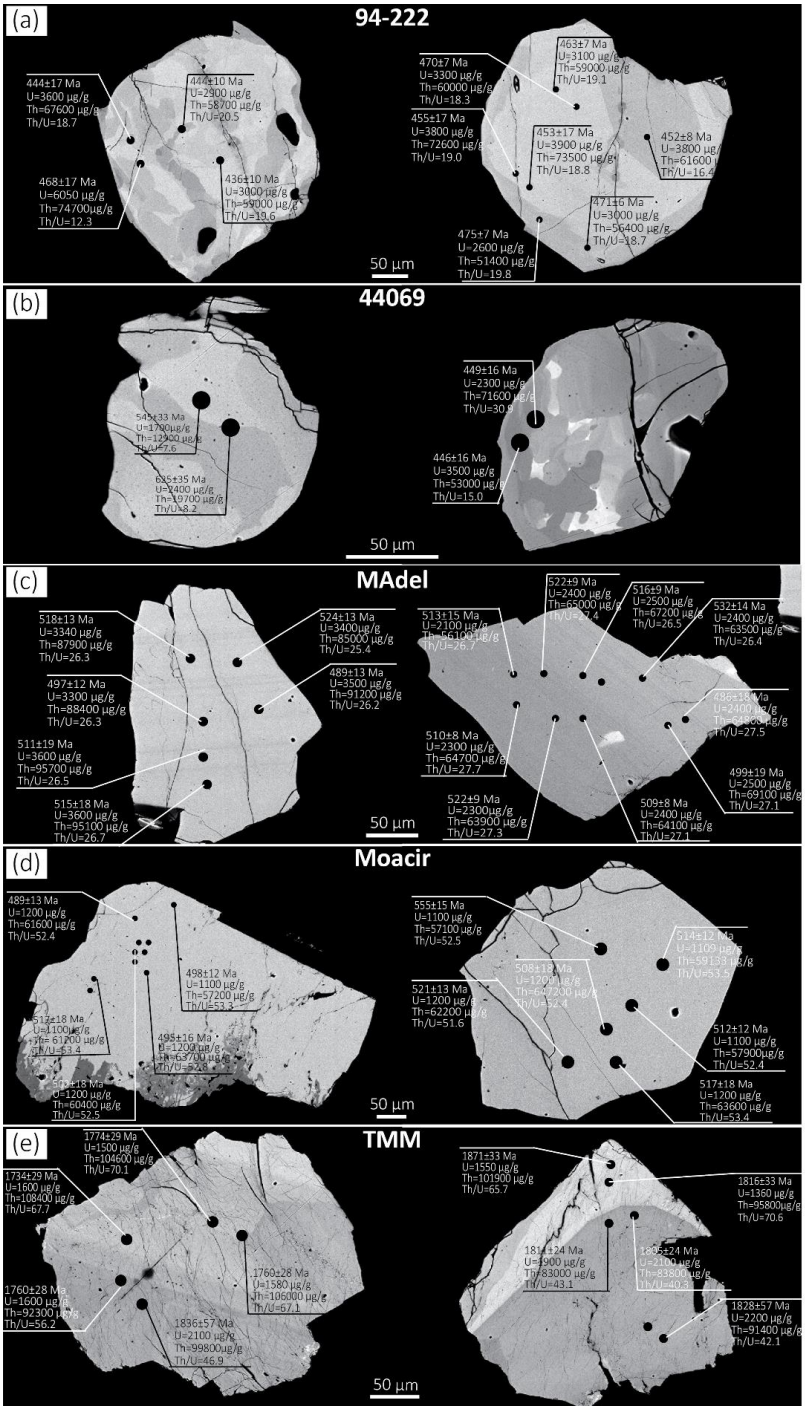

Figure 1. BSE images of the characteristic grains of monazite reference material (**a**) 94-222, (**b**) USGS

44069, (**c**) MAdel, (**d**) Moacir and (**e**) TMM showing different zoning patterns. The spots on the monazite grains represent the laser spots (spot size = 10 µm, repetition rate = 10 Hz) during four analytical sessions 120605, 130111, 130115 and 130320. It needs to be noted that solely the most distinctive monazite grains are shown here and not all grains analyzed, as well as laser spots. Furthermore, Th and U concentration (given in µg/g) and the calculated $^{206}Pb/^{238}U$ ages of each 10 µm spot on the monazite grain, shown here, are highlighted. Thorium and U concentrations were calculated from the count rates of ^{232}Th and ^{238}U and were normalized to the Th and U concentration of Moacir (Th = 6.92 wt.%; U = 0.13 wt.%; [55]). The correction factor based on the measured counts of Moacir relative to the Th and the U concentration given in µg/g (Th = 60810 µg/g and U = 1150 µg/g).

3.2. Analytical Set-Up and Sequence

LA-ICP-MS analyses were carried out in three different laboratories: (1) at the Institut für Geowissenschaften, Johannes Gutenberg-Universität Mainz (Germany), (2) at the Department of Earth Sciences, University of Gothenburg (Sweden) and (3) at the Isotopia Laboratory of the School of Earth, Atmosphere and Environment at Monash University in Melbourne (Australia). Instrumental set-up and operational parameters of each analytical session and the facility are summarized in Table 2. The LA-ICP-MS facility at Mainz is equipped with an ESI (Electro Scientific Industries, Inc., OR, USA) New Wave Research (NWR) 193 nm (ArF excimer) laser system and coupled to an Agilent 7500ce Quadrupole ICP-MS (Agilent Technologies, CA, USA). At the University of Gothenburg we applied a New Wave Research (NWR) 213 nm laser system combined with an Agilent 7500a series Quadrupole ICP-MS (Agilent Technologies, CA, USA) that is equipped with a secondary rotary pump. The carrier gas (Ar) was mixed with nitrogen (N_2) at a flow rate of 2 mL/min to slightly increase the signal intensity. The third facility, the Isotopia Laboratory, uses an ASI (Australian Scientific Instruments, ACT, Australia) RESOlution SE 193 nm ArF excimer laser equipped with a Laurin Technic S155 ablation cell coupled to a Thermo Fisher Scientific ICAP-Q.

Overall, eight analytical sessions (Table 2), which consists of a daily tuning routine, were undertaken. In each session, two to four runs with different operational settings were performed. Each run consisted of 25–30 spots in total, with 5–6 spots per sample. The calibration RM was measured two to three times in the beginning, after every 10 'unknowns' and at the end. During all eight analytical sessions, the ion intensities of ^{202}Hg, ^{204}Pb, ^{206}Pb, ^{207}Pb, ^{208}Pb, ^{232}Th and ^{238}U were measured. Data from the first two analytical sessions (120605, 130111) were used to (1) evaluate the effect of spot size and repetition rate on accuracy and precision of the U-Th/Pb age of the monazites and to (2) establish an analytical protocol that can be applied in different laboratories. The most commonly used analytical parameters for U-Th/Pb monazite dating such as a spot size (5, 10 and 20 µm) and repetition rate (5 and 10 Hz) were applied, e.g., [5,8,10,16,17,22,29,36,51,56]. To compare the results, the same ablation conditions were maintained by applying the same analytical setting and analyzing the same growth zone of the grains. During the first two analytical sessions, each spot was analyzed using a background, ablation time and washout time of 20, 30 and 20 s, respectively. To assess the differences in the absolute ages relative to ID-TIMS reference age, monazite USGS 44069 was used as calibration RM for all analytical sessions and runs, whereas the other RMs (TMM, MAdel, Moacir, 94-222) were treated as unknowns.

After determining suitable operational settings during the first two analytical sessions, the refinement of the ablation time to 15 s and the suitability of each individual RM was assessed in the third analytical session 130115, in which each RM was used as calibration RM by treating the others as unknown. This rotating roster allowed the assessment of each monazite against various absolute age calibrations and helps identify possible sources of absolute age biases in the reference ages. For example, when monazite 94-222 was used as calibration RM then USGS 44069, TMM, MAdel and Moacir were treated as unknowns.

The following five analytical sessions (130320, 130807, 130905, 160511 and 160606) were used to test the optimized operational parameter and its effect on obtained ages. All grains were analyzed with a spot size of 10 µm, a repetition rate of 10 Hz and a fluence of ~5.0 J/cm^2. Each spot was measured for

a total length of 55 s (20 s background, 15 s ablation, 20 s washout). An example of the ablation signal is shown in Figure 2. The first and the last 2.5 s of the peak signal were discarded. For the relative testing of instrumental set-ups, only monazite USGS 44069 was used as calibration RM for U-Th/Pb ages.

Table 2. Instrumental and operational settings for all eight analytical session.

Analytical Session	**120605**	**130111**	**130115**	**130320**	**130807**	**130905**	**160511**	**160606**
GENERAL INFORMATION								
Laboratory	Mainz	Gothenburg	Gothen-burg	Gothen-burg	Mainz	Mainz	Isotopia Laboratory	Isotopia Laboratory
ICP-MS series	Agilent 7500ce	Agilent 7500a	Agilent 7500a	Agilent 7500a	Agilent 7500ce	Agilent 7500ce	Thermo Fisher Scientific ICAP-Q	Thermo Fisher Scientific ICAP-Q
Laser model	ESI - ArF Excimer NWR 193, Two Vol 1 ablation cell	NWR 213, Two Vol ablation cell	NWR 213, Two Vol ablation cell	NWR 213, Two Vol ablation cell	ESI—ArF Excimer NWR 193, Two Vol 1 ablation cell	ESI—ArF Excimer NWR 193, Two Vol 1 ablation cell	ASI RESOlution SE 193 nm Laurin Technique S-155	ASI RESOlution SE 193 nm Laurin Technique S-155
OPERATIONAL SETTINGS								
Energy density	3.9–5.4 J/cm^2	4.2–5.7 J/cm^2	5.0 J/cm^2	4.8–5.1 J/cm^2	4.7–5.2 J/cm^2	4.8 J/cm^2	4.8–5.0 J/cm^2	4.8–5.0 J/cm^2
Repetition rate	5 Hz/10 Hz	10 Hz	10 Hz	10 Hz	10 Hz	10 Hz	10 Hz	10 Hz
Spot size	5 µm/10 µm/20 µm	5 µm/10 µm/ 20 µm	10 µm	10 µm	10 µm	10 µm	11 µm	11 µm
Background	20 s	20 s	15 s	12 s	20 s	20 s	20 s	20 s
Ablation time	30 s	30 s	15 s	15 s	15 s	15 s	15 s	15 s
Washout delay	15 s	10 s	15 s	15 s	20 s	20 s	20 s	20 s
INTEGRATION TIME								
^{202}Hg	0.03 s	0.03 s	0.03 s	0.03 s	0.03 s	0.03 s	0.03 s	0.03 s
^{204}Pb	0.03 s	0.03 s	0.03 s	0.03 s	0.03 s	0.03 s	0.03 s	0.03 s
^{206}Pb	0.04 s	0.04 s	0.04 s	0.04 s	0.04 s	0.04 s	0.04 s	0.04 s
^{207}Pb	0.06 s	0.06 s	0.06 s	0.06 s	0.06 s	0.06 s	0.06 s	0.06 s
^{208}Pb	0.01 s	0.02 s	0.02 s	0.02 s	0.02 s	0.02 s	0.02 s	0.02 s
^{232}Th	0.01 s	0.01 s	0.01 s	0.01 s	0.01 s	0.01 s	0.01 s	0.01 s
^{238}U	0.01 s	0.01 s	0.01 s	0.01 s	0.01 s	0.01 s	0.01 s	0.01 s

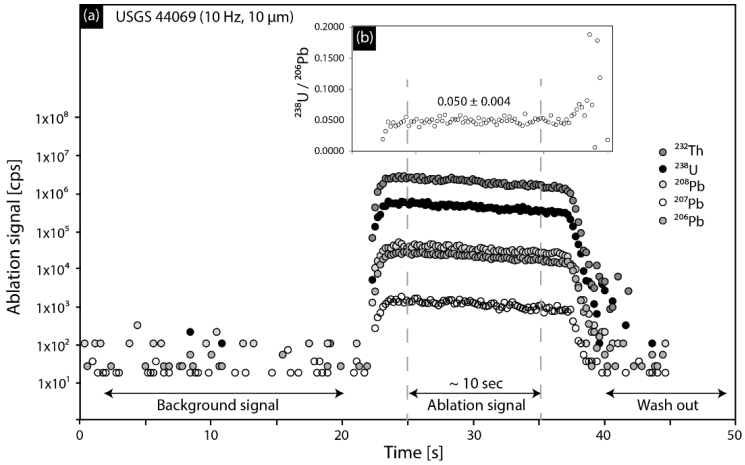

Figure 2. Typical time-resolved (**a**) ablation signal for a 10 µm spot at 10 Hz repetition rate of the calibration RM USGS 44069 (analytical session 130807, Uni Mainz) in counts per second (cps) for all isotopes measured. The ablation signal consists of ~20 s background measurement, ~15 s ablation signal and the first 5 s of the wash out time. The two vertical grey dashed lines within the ablation signal indicate the used signal for data reduction. Plot (**b**) shows the ^{238}U/^{206}Pb ratio of the ablation signal of the same spot analysis. The value represents the mean of the ratio ±1 RSD uncertainty.

3.3. Instrumental Data Assessment and Age Calculations

Raw data from the mass spectrometer were reduced and evaluated using the Iolite 3 software [57,58] and an accompanying in-house (University of Gothenburg) Microsoft Excel™ spreadsheet. Notable is that the in-house Excel spreadsheet uses raw data ratios without baseline correction compared to the Iolite software. The Iolite data reduction scheme applied here was 'U-Pb geochron4'. Both data reduction schemes, the in-house Excel-spreadsheet and the Iolite DRS do not apply a common-Pb correction. The reduced data and results from both data reduction methods are provided in Tables S1–S3 in supplementary materials and Figure 3.

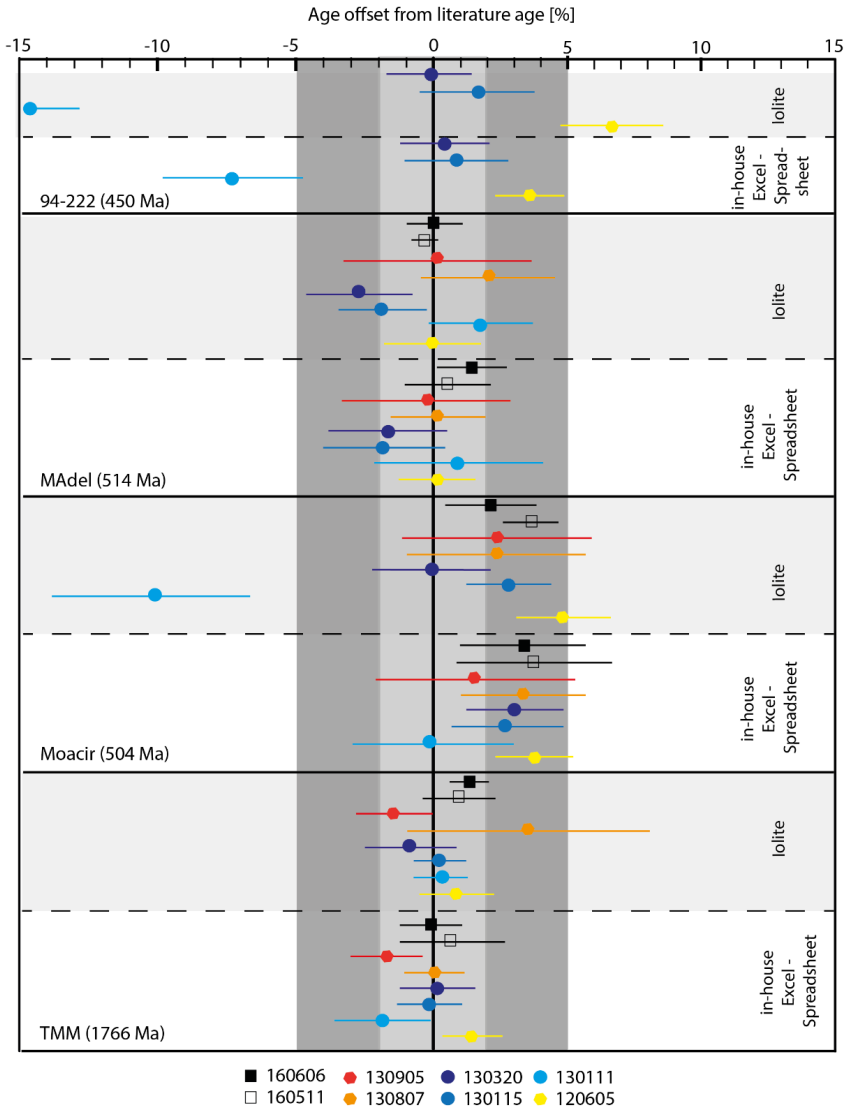

Figure 3. Comparison of the concordia ages calculated from the final ratios from the Iolite software and the in-house Excel worksheet, for monazite RM 94-222, Madel, Moacir and TMM. Monazite USGS 44049 was used as calibration RM and is therefore not displayed. Each spot/square represents the offset of the calculated concordia age from the literature value for a certain analytical session. The uncertainties are given in 2s. The light grey and dark grey bars represent the overall offset in per cent achieved in this study with 2% and 5%, respectively. Concordia data from the in-house Excel-spreadsheet is given in Table 3. All other data, the calculated concordia ages from the Iolite reduced data, the reduced data from the in-house spreadsheet and the Iolite software are provided in Table S2 and Table S3. It needs to be noted that the large discrepancy for monazite sample 94-222 in analytical session 130111 could be of analytical nature or due to data reduction. The exact reason for this offset, however, remains unknown.

In the following, the data reduction of the in-house Microsoft Excel^{TM} worksheet is briefly explained. The U-Th/Pb age calculation is based on the mean count rates of each measured isotope. The age and corresponding uncertainty, expressed as the standard deviation (SD) and the relative standard error (RSE), of each spot were calculated for $^{208}Pb/^{232}Th$, $^{207}Pb/^{235}U$, $^{206}Pb/^{238}U$ and $^{207}Pb/^{206}Pb$. The ^{235}U, for monazite samples TMM, MAdel and 94-222, were calculated from ^{238}U by using the widely accepted $^{238}U/^{235}U$ value of 137.88 [59], whereas for the monazite reference sample USGS 44069 and Moacir, the recently characterized $^{238}U/^{235}U$ value of 137.856 and 137.743 was used [60]. However, it needs to be noted that the relative uncertainty and natural variations in U isotope compositions, i.e., < 0.1%, are negligible with respect to the external precision of the method [13].

All ^{208}Pb-^{232}Th, ^{207}Pb-^{235}U, ^{206}Pb-^{238}U and ^{207}Pb-^{206}Pb ages were calculated using the 'raw' isotopic ratios, here defined as the isotopic ratios without background subtraction. The same time slice for the sample and the RM was used to account for a systematic change in isotopic ratios as course of fractionation [61,62]. The isotopic ratio is based on circa 10 s ablation time for all analytical sessions, even though the ablation time of the analytical sessions 120605 and 130111 was set to 30 s (Table 1). Outliers in the peak signal that deviated by more than 2 RSD from the mean count rate of each isotope were not considered in the data reduction. To calculate the U-Th/Pb monazite ages, the mean measured ratio of each spot is normalized to a correction factor that is based on the measured ratio of all the analyzed USGS 44069 (calibration RM) relative to the preferred ratio calculated for the given TIMS $^{206}Pb/^{238}U$ age of [424.9 ± 0.8 Ma, 19]. The correction factor was calculated for each individual analytical session and run. Reported uncertainty is calculated by propagating uncertainties (e.g., RSE) of each monitored isotope within the selected time span of the peak given at the 95% confidence level (2s). The uncertainty propagation and elemental ratio calculation followed the calculation described by [63]. Ultimately, individual U/Pb concordia and $^{208}Pb/^{232}Th$ weighted mean ages have been calculated using Isoplot 4.15 [64]. No common Pb-correction was performed, due to the negligible common Pb and concordant ages of the monazite samples analyzed in this study.

4. Results and Discussion

4.1. Optimisation of Running Parameters

Firstly, we compare the results of the different running parameters from analytical sessions 120506 and 130111 using monazite USGS 44069 as a calibration RM. Data from the in-house Excel-spreadsheet is used for the comparison. The results from the first two analytical sessions (120605 and 130111) show that with a spot size of 10 µm and a repetition rate of 10 Hz a precision (here defined as the age uncertainty) of ±2.5% is achieved for U/Pb ages. The absolute age is within ± 2.0% of the U/Pb concordia age. For Th/Pb ages the precision is lower with ±3.7%, but accuracy is still maintained.

Neither a smaller (5 µm) nor a larger (20 µm) spot size yield an improvement on the precision, leading to the conclusion that the spot size of 10 µm and a repetition rate of 10 Hz are the best operational settings. Whilst all analyses show systematic variations in reproducibility with spot size and/or parent-daughter ratio, all ages remain accurate, which indicates that even a 5 µm spot can be used to date monazite grains.

In addition to this, to optimize running parameters, the correction factor, here defined as the average measured ratio of the RM relative to the preferred ratio calculated for the given literature age, needs to be monitored and assessed. To do so, the correction factors from each run of analytical session 120605 were evaluated. In general, the correction factor should be ~1, but the data obtained from this run shows that the correction factor increases with increasing spot sizes from 5 µm to 20 µm (Table 3 and Figure 4). This is especially true for ratios including two different elements (e.g., $^{206}Pb/^{238}U$). Notable is that between 10 µm and 20 µm the change in correction factor is less pronounced. Thus, the results allow two different interpretations. Firstly, it appears to be tolerable to analyze the RM and the unknown by using slightly different spot sizes, but only when small variations in correction factor occur, e.g., for larger spot sizes (> 15 µm, Figure 4 and Table 3).

Secondly, based on the variation between the spot size and the applied correction factor (Figure 4), accurate U-Th/Pb ages within ±2.0% from the ID-TIMS age can be determined for a spot size as small as 10 µm, repetition rate of 10 Hz and a fluence of ~5.0 J/cm^2. The precision and accuracy of the determined age of this study is similar to results from the study of [10] that used a lower limit of 8 µm and 10 J/cm^2 at 5 Hz. Combining all eight analytical sessions, the overall precision obtained here by using 10 µm and 10 Hz results in an average reproducibility of ±1.6% and ±3.0% for U/Pb concordia and for Th/Pb ages, respectively.

With the largest spot size applied in this study (20 µm), absolute ages of this study differ from the reference ages determined by ID-TIMS by, on average, 2.0%. The somewhat better within-analytical session run precision of ± 0.7% may reflect the higher counting rates but is dwarfed by the bias in data and thus cannot be applied to maintain accuracy.

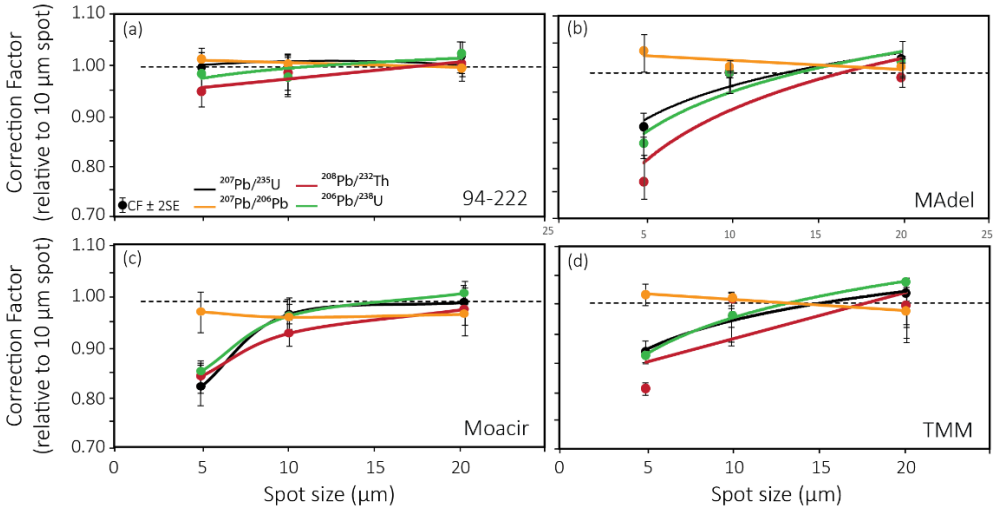

Figure 4. Correction factor versus spot size relative to 10 µm and 10 Hz of monazite sample USGS 44069 of analytical session 120605. The graph shows Th/Pb, U/Pb and Pb/Pb fractionation factors for (**a**) 94-222, (**b**) MAdel, (**c**) Moacir and (**d**) TMM. The dashed line represents the line at which the average measured ratio of the RM relative to the preferred ratio calculated for the given literature age should be equal. The bold colored line represents the calculated trendline for each decay system. The uncertainty is given in 2SE of the mean of all analyses of this run. The Pb/Pb, Th/Pb and U/Pb is similar for all samples.

The differences of U/Pb with varying spot size and a different repetition rate observed in analytical session 120605 are most likely related to isotopic fractionation in the pit (Figure 4 and Figure S1). Using a small spot size (5 µm) and a low repetition rate (5 Hz) by maintaining low energy (5.0 J/cm^2) results in a deviation from the literature U/Pb concordia ages of about ± 5% and a precision of ± 4.5% for all measured RM, whereas with a higher repetition rate of 10 Hz the difference is nearly halved (± 2%) with an age uncertainty of ± 3% (Table 3). The difference between U-Th vs Pb being ejected from the crater are thus paramount in obtaining accurate ages. To obtain accurate ages it is therefore important that a balance between repetition rate energy of the laser beam is maintained. However, according to [10], U/Pb and Th/Pb are more likely to reflect true ratios when using larger spot sizes. Thus, a balanced spot size versus count rate ratio needs to be chosen to ensure highly precise analyses and to minimize the destruction of the monazite sample.

Table 3. Concordia and $^{208}Pb/^{232}Th$ weighted mean age of 94-222, USGS 40069, MAdel, Moacir and TMM monazite reference samples of each analytical session. The ages presented in this table have been evaluated and reduced using the in-house Excel spreadsheet. Concordia and $^{208}Pb/^{232}Th$ weighted mean age obtained using the Iolite software is presented in Table S2 and Table S3. Monazite sample USGS 44069 has been used as calibration RM. The uncertainty is given in 2s. The number of spots analyzed is given 'n'. Data of each spot are provided in Table S1.

Monazite Reference Sample	Analytical Session	Spot Size [µm]	Repetition Rate [Hz]	Concordia Age						$^{208}Pb/^{232}Th$ Weighted Mean Age					
				Age [Ma]	2s	Age Uncertainty	Deviation from Literature Value	MSWD	Probability	Age [Ma]	2s	Age Uncertainty	Deviation from Literature Value	MSWD	Probability
94-222	*120605*	5	5	471	18	3.8%	4.7%	0.02	0.89	463	12	2.6%	2.9%	0.53	0.76
		5	10	456	14	3.1%	1.3%	0.38	0.54	474	12	2.5%	5.3%	0.22	0.95
		10	10	466	6	1.3%	3.6%	0.51	0.47	466	8	1.6%	3.6%	0.10	0.96
		20	10	452	9	2.0%	0.4%	0.02	0.88	434	8	1.8%	3.6%	1.20	0.30
	130111	5	10	405	16	4.0%	11.1%	1.12	0.29	425	13	3.1%	5.9%	0.35	0.89
		10	10	419	11	2.6%	7.4%	2.30	0.13	420	15	3.6%	7.1%	0.12	0.99
		20	10	445	13	2.9%	1.1%	0.09	0.76	405	13	3.2%	11.1%	0.14	0.98
	130115	10	10	454	8	1.9%	0.9%	3.90	0.048	445	8	1.9%	1.1%	0.54	0.90
	130320	10	10	452	8	1.7%	0.5%	2.30	0.13	452	7	1.6%	0.5%	0.26	0.98
MAdel	*120605*	5	5	542	23	4.2%	5.4%	0.42	0.52	534	16	3.0%	3.9%	0.95	0.44
		5	10	521	18	3.5%	1.4%	2.50	0.12	543	15	2.8%	5.6%	0.79	0.53
		10	10	515	7	1.4%	0.2%	0.00	0.98	515	8	1.6%	0.2%	0.43	0.78
		20	10	515	12	2.3%	0.2%	1.50	0.22	505	11	2.2%	1.8%	0.52	0.72
	130111	5	10	546	25	4.6%	6.2%	0.04	0.85	595	26	4.4%	15.8%	0.28	0.89
		10	10	519	16	3.1%	1.0%	3.40	0.07	533	20	3.8%	3.7%	0.04	0.99
		20	10	502	18	3.6%	2.3%	3.30	0.07	481	22	4.6%	6.4%	0.07	0.93
	130115	10	10	505	11	2.2%	1.8%	2.60	0.11	500	11	2.2%	2.7%	0.16	1.00
	130320	10	10	506	11	2.2%	1.6%	0.80	0.37	504	10	2.0%	1.9%	1.40	0.23
	130807	10	10	515	10	1.8%	0.2%	0.47	0.49	516	14	2.7%	0.4%	0.37	0.78
	130905	10	10	513	16	3.1%	0.2%	0.15	0.70	526	28	5.3%	2.3%	0.03	0.99
	160511	11	10	517	8	1.6%	0.6%	0.75	0.39	507	9	1.7%	1.4%	0.02	1.00
	160606	11	10	522	7	1.3%	1.5%	6.60	0.01	519	8	1.5%	1.0%	0.19	0.94

Table 3. *Cont.*

Monazite Reference Sample	Analytical Session	Spot Size [μm]	Repetition Rate [Hz]	Concordia Age						$^{208}Pb/^{232}Th$ Weighted Mean Age					
				Age [Ma]	2s	Age Uncertainty	Deviation from Literature Value	MSWD	Probability	Age [Ma]	2s	Age Uncertainty	Deviation from Literature Value	MSWD	Probability
Moacir	*120605*	5	5	524	22	4.2%	4.0%	0.02	0.88	501	14	2.8%	0.6%	2.20	0.06
		5	10	520	17	3.3%	3.2%	0.03	0.87	509	12	2.4%	1.0%	1.80	0.11
		10	10	523	7	1.4%	3.8%	3.90	0.048	524	25	4.8%	4.0%	2.90	0.03
		20	10	517	12	2.3%	2.6%	5.60	0.02	481	34	7.1%	4.8%	6.70	0.00
	130111	5	10	529	26	4.9%	5.0%	0.00	0.96	555	25	4.5%	10.1%	0.29	0.89
		10	10	504	15	3.0%	0.0%	2.10	0.15	507	18	3.6%	0.6%	0.06	0.99
		20	10	491	19	3.9%	2.6%	2.70	0.10	464	19	4.1%	8.6%	0.14	0.94
	130115	10	10	518	11	2.1%	2.8%	1.01	0.32	512	12	2.3%	1.6%	0.46	0.90
	130320	10	10	520	9	1.8%	3.1%	3.10	0.08	503	13	2.6%	0.2%	2.00	0.03
	130807	10	10	521	12	2.3%	3.4%	3.10	0.08	523	13	2.5%	3.8%	2.00	0.09
	130905	10	10	512	19	3.7%	1.6%	0.03	0.85	530	34	6.4%	5.2%	0.14	0.87
	160511	11	10	523	15	2.9%	3.8%	1.01	0.31	511	12	2.3%	1.4%	0.01	0.998
	160606	11	10	521	12	2.3%	3.4%	1.6	0.21	518	8	1.6%	2.7%	0.55	0.65
TMM	*120605*	5	5	1708	47	2.8%	3.4%	3.00	0.08	1656	48	2.9%	6.6%	0.16	0.96
		5	10	1743	44	2.5%	1.3%	0.06	0.81	1769	44	2.5%	0.2%	0.39	0.81
		10	10	1792	20	1.1%	1.5%	2.70	0.10	1762	27	1.5%	0.2%	0.90	0.46
		20	10	1786	37	2.1%	1.1%	4.60	0.03	1726	40	2.3%	2.3%	0.94	0.44
	130111	5	10	1673	69	4.1%	5.6%	13.00	0.00	1644	66	4.0%	7.4%	0.32	0.86
		10	10	1735	31	1.8%	1.8%	1.60	0.21	1622	54	3.3%	8.9%	0.06	0.99
		20	10	1740	19	1.1%	1.5%	0.43	0.51	1602	56	3.5%	10.2%	0.39	0.82
	130115	10	10	1764	21	1.2%	0.1%	14.00	0.00	1703	40	2.3%	3.7%	0.23	0.99
	130320	10	10	1769	25	1.4%	0.2%	0.09	0.76	1812	71	3.9%	2.6%	2.20	0.05
	130807	10	10	1767	19	1.1%	0.1%	0.20	0.66	1752	36	2.1%	0.8%	0.92	0.47
	130905	10	10	1736	23	1.3%	1.7%	0.89	0.35	1739	75	4.3%	1.6%	0.08	1.00
	160511	11	10	1778	35	2.0%	0.7%	0.24	0.62	1502	75	5.0%	17.6%	0.19	0.83
	160606	11	10	1766	19	1.1%	0.0%	3.8	0.05	1834	27	1.5%	3.7%	0.31	0.82

4.2. Analytical and Inter-Lab Comparison for U-Th/Pb Dating of Monazite

In addition to the operation condition, instrumental characteristics may have an effect on age determinations, too. To investigate this, monazite sample Moacir was chosen to evaluate the count rate statistics between the three different laboratories and all eight analytical sessions. Moacir was chosen because of being the most homogeneous monazite sample compared to USGS-44069, TMM, MAdel or 94-222 (Figure 1). The LA-ICP-MS instruments at the Institute of Geoscience in Gothenburg (Agilent 7500a) and School of Earth, Atmosphere and Environment at Monash University Melbourne, (ThermoFisher Scientific ICAP-Q) obtain two to four times higher count rates (Figure 5) with the same repetition rate and spot size than at the facility in Mainz (Agilent 7500ce). The lowest count rates in this study were achieved at Mainz where the ICP-MS is equipped with one rotary pump and only Ar and He are used as carrier gas. The signal size at the other two facilities, Gothenburg and Monash University, were about four times higher for the same RM, which can be attributed to the second rotary pump that can create a better vacuum within the analyzer region of the ICP-MS, between the sample cone and the ion extraction lens [65], and the addition of N_2 to the carrier gas (Ar, He), which increases the plasma temperature and its ionizing efficiency [65,66]. Having stated that, different instrumental set-up and minor adjustments in the operational set-up that enhances the sensitivity leads to the same accuracy of the concordia and Th/Pb ages (< ± 2%) of all analyzed monazite samples in all facilities.

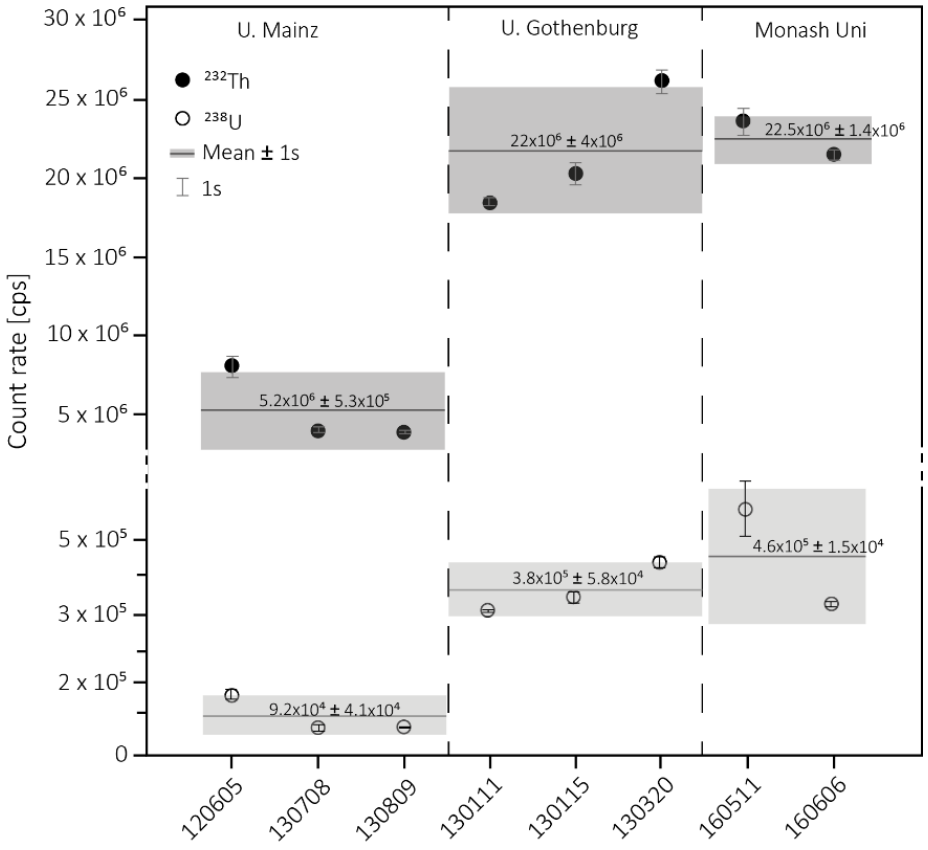

Figure 5. Comparison of the ^{238}U and ^{232}Th count rates of monazite reference sample Moacir obtained in the three LA-ICP-MS laboratories using a spot size of 10 µm and a repetition rate of 10 Hz. In analytical sessions 120605, 130111, 130115 and 130320 the same monazite grains were analyzed, whereas in analytical sessions 130807 and 130905 and in analytical sessions 160511 and 160606 different Moacir grains from the same sample batch were analyzed.

4.3. Evaluation of Monazite Reference Samples

4.3.1. Chemical Homogeneity

All of the five analyzed monazite samples show different zoning patterns, such as patchy (Figure 1, a left, b right), oscillatory (Figure 1c, right) and concentric (Figure 1, a right, e right). Some grains may also contain mineral inclusions (for example Moacir, Figure 1d), which will compromise data reproducibility substantially. Patchy patterns in monazite grains, such as the USGS 44069 monazite grain, may be the result of recrystallization processes [67–69] or reflect the exsolution of Huttonite and Cheralite [24,70]. These may not affect U/Pb dating, depending on the timing and nature of their origin. Indeed, even though small Th and U concentration variations occur within the grains, it appears that the effect on U/Pb and Th/Pb ages is negligible. Monazite sample MAdel and Moacir are good RMs for trace element calibrations as they appear homogeneous with minor oscillating chemical zonation, whereas TMM, USGS 44069 and 94-222 show strong chemical zoning with variable Th and U concentrations (Figure 1).

4.3.2. Precision and Accuracy of the U-Th/Pb Ages

The U-Th/Pb age data of the third analytical session 130115 was used to assess the suitability of the RM by comparing ages of each analyses against one monazite that acts as a calibration RM. This calibration RM is rotating, which allows a cross-calibration of all RMs relative to each other. The coherency of results, also in comparison with reference values determined by ID-TIMS, reveals the suitability as a RM. Figure 6 shows calculated ages of each monazite, its associated literature age and the uncertainty ellipses of the respective RM that was used to calculate the age. The results show that all but one monazite appears suitable as a primary age RM. When using monazite USGS 44069 and 94-222 as calibration RM, the ages of the respective reference monazite, tested in this study, are within the uncertainty of the published ages. When using MAdel as calibration RM, the calculated U-Th/Pb ages get systematically older but remain within uncertainty of the literature ages. When the oldest monazite sample, TMM, is used as the calibration RM, the results for some of the other tested RMs tend to scatter with a higher uncertainty, but the calculated ages still overlap with their published ages (Figure 6). The only RM that yields inconsistent ages is monazite sample Moacir, with U/Pb concordia ages and Th/Pb ages appearing significantly (by 4%) older than the proposed 504 ± 0.2 Ma age [31] in the literature.

Figure 6a shows that when using USGS 44069, MAdel and TMM as calibration RM for Moacir, the mean concordia age results in 517 ± 15 Ma (2s). Even though within uncertainty of the reference age, the substantially older mean calculated age indicates a systematic bias from the other three RMs that strongly argues for an older formation age of the analyzed Moacir fragments. Indeed, we could not reproduce the published SHRIMP $^{206}Pb/^{238}U$ age of 474 Ma [20] nor the re-calibrated $^{207}Pb/^{235}U$ ID-TIMS age of 504 Ma [31] when using USGS 44069 or the other RMs as a calibration RM (Figure 6a). As discussed in [48], the $^{207}Pb/^{235}U$ TIMS age [31] does not overlap within uncertainty of the previously reported SHRIMP age, which could be 'an inter-laboratory' analytical artefact. However, the re-calibrated $^{206}Pb/^{238}U$ ID-TIMS age of 516 Ma [21] is in good agreement with the results of this study. Figure 7 shows that $^{208}Pb/^{232}Th$ (0.02577 ± 0.0008) and $^{206}Pb/^{238}U$ (0.08329 ± 0.0027) give similar ages within the analytical uncertainty of 514.1 ± 3.9 (2s) and 517.6 ± 4.2 (2s), respectively. The calculated $^{206}Pb/^{238}U$, $^{207}Pb/^{235}U$ and $^{208}Pb/^{232}Th$ ages of this study are all identical with the $^{206}Pb/^{238}U$ ID-TIMS age of [21], all agreeing within analytical uncertainty of ± 2%. We, therefore, propose that the TIMS age of 517 Ma [21] is a suitable reference age for monazite sample Moacir. However, our mean concordia age for Moacir is 520 ± 3.9 Ma (2s, Figure 7d). This age is calculated from all eight analytical sessions using the reduced ratios from the in-house Excel spreadsheet from all runs with a spot size of 10 µm and 10 Hz. The calculated concordia age broadly agrees with the value of [21] even though it is on the upper end.

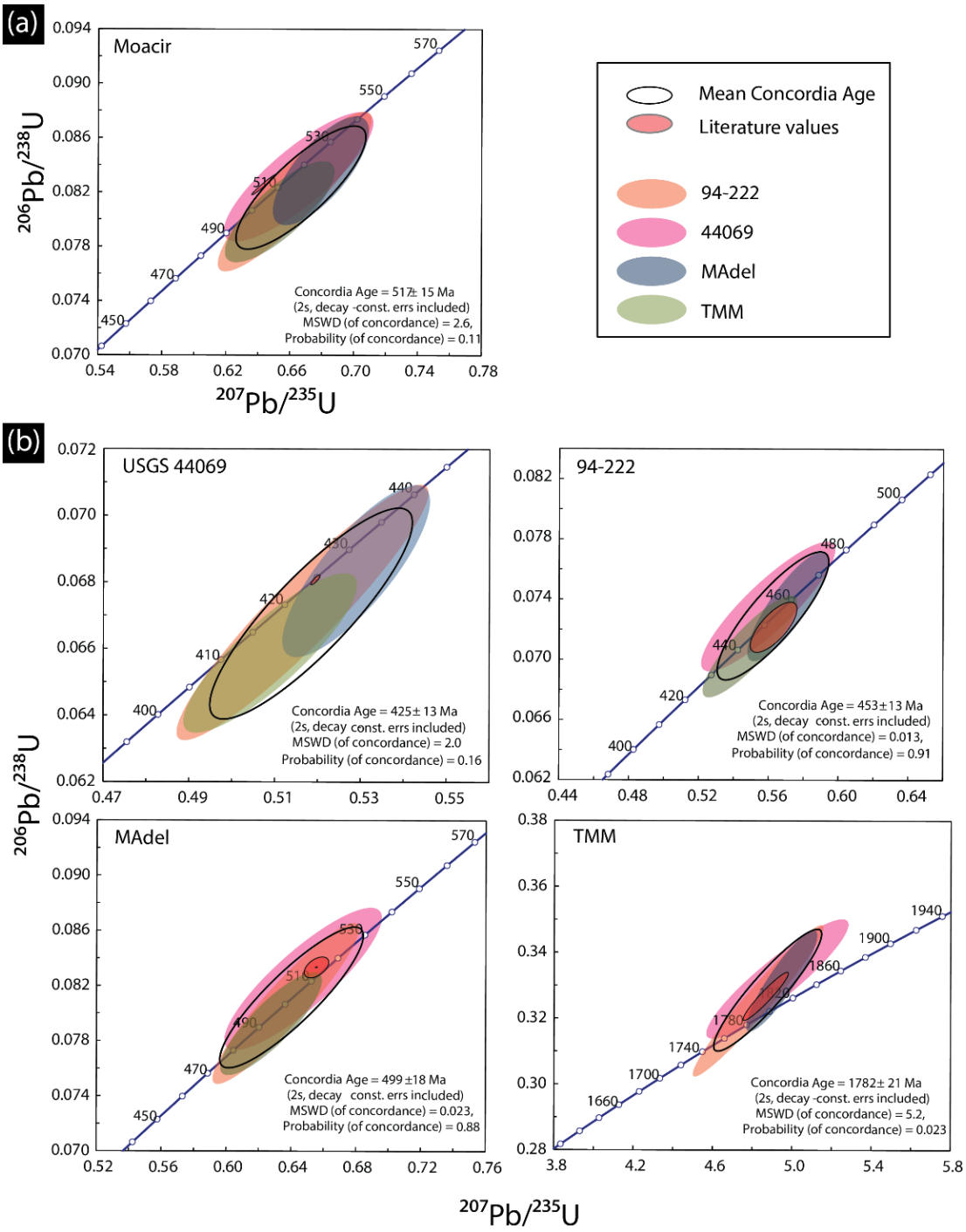

Figure 6. Accuracy plots after [71]. The data (Table S4) for this calculation were used from the analytical session 130115. Each ellipse represents the age of monazite as standardized with a different monazite. For example, the orange ellipse in the USGS 44069 accuracy concordia plot represents the age of USGS 44069 normalized to 94-222. The given concordia age results from all ellipses plotted in the graph. The ellipses represent 2s uncertainty. The red data ellipse shows the literature value. (**a**) Accuracy plot for Moacir (n = 10) shows that the mean concordia age does not overlap with the literature value. Due to this, we excluded Moacir from all other plots, because the accuracy and precision would be reduced for the tested RMs. (**b**) Accuracy plots for monazite reference sample USGS 44069 (n = 12), 94-222 (n = 14), MAdel (n = 10) and TMM (n = 9).

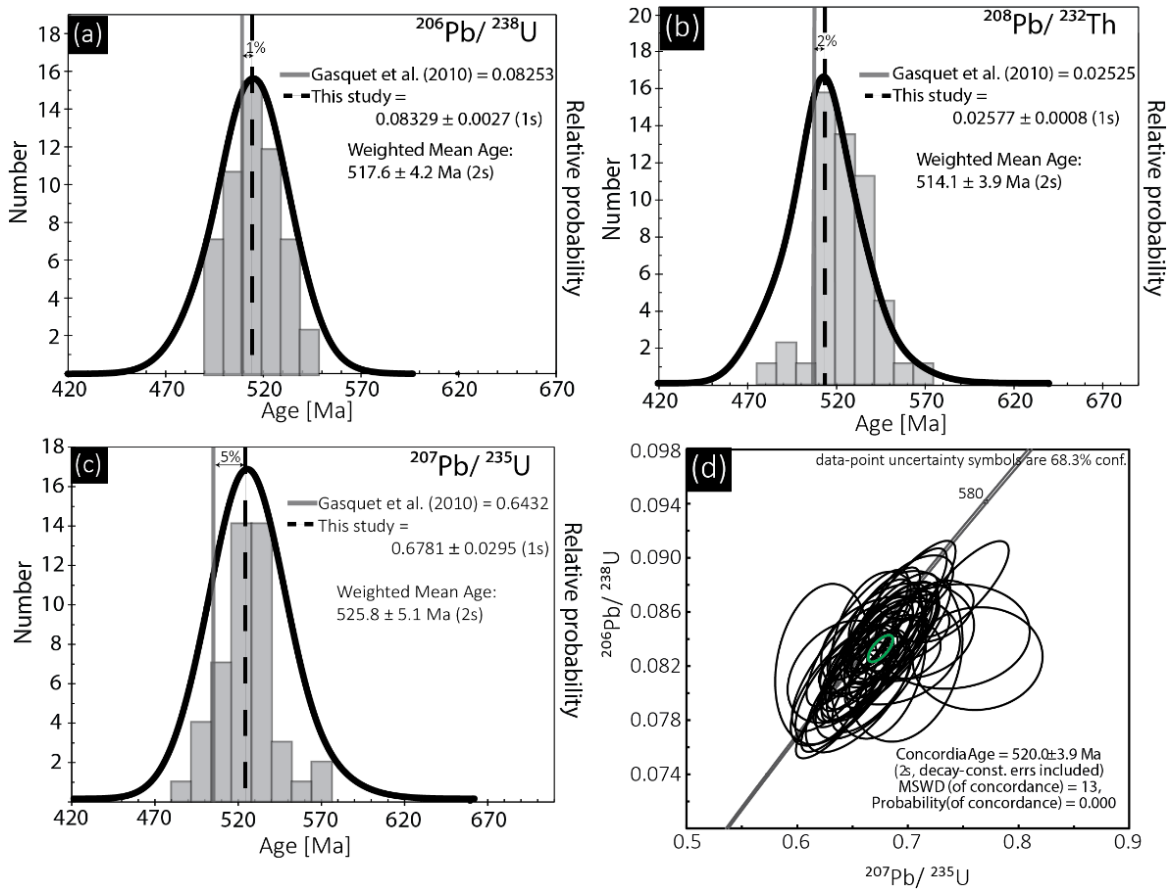

Figure 7. Relative probability plots [using Isoplot add-in for Excel, 64]) for (**a**) $^{206}Pb/^{238}U$ (n = 54), (**b**) $^{208}Pb/^{232}Th$ (n = 51) and (**c**) $^{207}Pb/^{235}U$ (n = 46) ages of all analytical sessions from this study using a spot size of 10 µm and a repetition rate of 10 Hz compared to published U-Th/Pb ages of [31]. For each plot the ratios and weighted mean age are given. [31] published a $^{206}Pb/^{238}U$ age of 511.2 ± 0.4 Ma, which corresponds to a ratio of 0.08253 and a $^{208}Pb/^{232}Th$ age of 504 Ma corresponding to a ratio of 0.02525. The $^{207}Pb/^{206}Pb$ (0.056824 ± 0.072%), $^{207}Pb/^{235}U$ (0.64831 ± 0.13%) and $^{206}Pb/^{238}U$ (0.082830 ± 0.064%) of [21] are within analytical uncertainty. Graph (**d**) shows the concordia plot with the suggested age of Moacir.

5. Conclusions

Ablation conditions during LA-ICP-MS analyses (laser spot size, repetition rate, laser fluence) can affect the resulting ages for monazite U-Th/Pb geochronology. We suggest a spot size of 10 µm, a repetition rate of 10 Hz and a laser fluence of 5 J/cm^3 as optimal running conditions, under which a precision of ±2% is achieved and ages are obtained within uncertainty of reported high precision ID-TIMS ages. A smaller laser spot diameter still yields accurate results, yet with poorer precision, indicating that increasing sensitivity in future studies can achieve higher precisions with higher spatial resolution. The results further demonstrate that USGS 44069, 94-222, Madel and TMM are suitable as monazite RMs for U-Th/Pb dating. Caution is advised for the use of Moacir as an RM. The reason for differences in reported ages for Moacir remains to be explored and a 'true' age needs to be determined. However, our iterative approach indicates a plausible U/Pb age of ~517 Ma, for the monazite grains analyzed in this study.

Supplementary Materials: The following are available online at http://www.mdpi.com/2076-3263/9/9/391/s1. Figure S1. Correction factor for each U-Th/Pb ratio relative to USGS 44069 for 10 µm and 10 Hz of analytical session 120605 for all monazite RMs. The correction factor for U-Th/Pb remains the same for each monazite analysed. The uncertainty of the Th/Pb and U/Pb correction factor ranges between 2% to 4%, whereas for Pb/Pb it only varies by 1%, indicating that each monazite sample tested here is suitable as calibration RM. Attention has to be paid using Moacir due to age uncertainties. Table S1: U/Pb and Th/Pb data (age and raw ratios) of all runs for each monazite reference sample. Data shows the U-Th/Pb data of the in-house Excel spreadsheet. *Analytical sessions (120605, 130807, 130905) were carried out at the Johannes Gutenberg-University, Mainz, Germany. **Analytical sessions (130111, 130115, 130320) were carried out at the University, Gothenburg, Sweden. ***Analytical sessions (160511, 160606) were carried out at Monash University, Melbourne, Australia; (1) Uranium and Thorium concentrations were calibrated on the RM Moacir (Seydoux-Guillaume et al., 2004) accepted values are U = 1150 µg/g and Th = 60810 µg/g. Th/U ratio results from the given Th and U content. (2) Total common Pb in sample. (3) Ratios were calculated from initial values and were calibrated on RM USGS 44069 (Aleinikoff et al., 2006). (4) Uncertainty is calculated from initial values and calibrated using USGS 44069 (Aleinikoff et al., 2006). (5) Rho – uncertainty correlation between $^{207}Pb/^{235}U$ and $^{206}Pb/^{238}U$. (6) Ages were calculated after U-Th/Pb equation after principles of the radioactive decay equation. Decay constants used for calculation $^{238}U = 0.155125 \times 10^{-9}$ y^{-1}, $^{235}U = 0.98485 \times 10^{-9}$ y^{-1} and $^{232}Th = 0.049475 \times 10^{-9}$ y^{-1} [1] (8) Uncertainty is calculated from initial values after principles of the radioactive decay equation. Table S2: U/Pb and Th/Pb data (age and raw ratios) of all runs for each monazite reference sample. Data shows the Iolite reduced U-Th/Pb ages and ratios. *Analytical sessions (120605, 130807, 130905) were carried out at the Johannes Gutenberg-University, Mainz, Germany. **Analytical sessions (130111, 130115, 130320) were carried out at the University, Gothenburg, Sweden. ***Analytical sessions (160511, 160606) were carried out at Monash University, Melbourne, Australia; (3) Ratios were calculated from initial values and were calibrated on RM USGS 44069 (Aleinikoff et al., 2006). (4) Uncertainty is calculated from initial values and calibrated using USGS 44069 (Aleinikoff et al., 2006). (5) Rho – uncertainty correlation between $^{207}Pb/^{235}U$ and $^{206}Pb/^{238}U$. (6) Ages were calculated after U-Th/Pb equation after principles of the radioactive decay equation. Decay constants used for calculation $^{238}U = 0.155125 \times 10^{-9}$ y^{-1}, $^{235}U = 0.98485 \times 10^{-9}$ y^{-1} and $^{232}Th = 0.049475 \times 10^{-9}$ y^{-1} [1] (8) Uncertainty is calculated from initial values after principles of the radioactive decay equation. Table S3. Concordia age of 94-222, USGS 40069, MAdel, Moacir and TMM monazite reference samples of all analytical sessions. The ages presented in this table have been evaluated and reduced using the Iolite data reduction scheme 'U-Pb geochron4'. Monazite RM USGS 44069 was used as calibration RM. The uncertainty is given in 2s. The number of spots analyzed is given 'n'. Data of each spots are provided in Supplementary Table S2. Table S4: Mean U/Pb ratios and uncertainties used for Figure 6. The average for each monazite RMs does not include the Moacir values due to low precision and accuracy.

Author Contributions: M.R. (Marianne Richter). acquired data and wrote the first draft of the manuscript. Y.N.-J. and O.N. helped with interpretation and manuscript preparation. D.R. and T.Z. acquired the samples. T.Z., R.M.-K. and M.R. (Massimo Raveggi). helped with the analytical set-up. All authors contributed to the editing of the manuscript.

Funding: M.R. (Marianne Richter) was supported by a postgraduate scholarship of Monash University and the SEAE.

Acknowledgments: We would like to thank Justin Payne, John Aleinikoff, Anna-Magali Seydoux-Guillaume and Daniela Rubatto for providing the monazite reference samples for this project. MRI acknowledges Estephany Marillo-Sialer for her help with Iolite and Stephan Buhre for his help with the BSE imaging at the JGU in Mainz.

Conflicts of Interest: The authors declare no conflicts of interest.

References

1. Clavier, N.; Podor, R.; Dacheux, N. Crystal chemistry of the monazite structure. *J. Eur. Ceram. Soc.* **2011**, *31*, 941–976. [CrossRef]
2. Engi, M. Petrochronology based on ree-minerals: Monazite, allanite, xenotime, apatite. *Rev. Mineral. Geochem.* **2017**, *83*, 365–418. [CrossRef]
3. Spear, F.S.; Pyle, J.M. Apatite, monazite and xenotime in metamorphic rocks. *Rev. Mineral. Geochem.* **2002**, *48*, 293–335. [CrossRef]
4. Parrish, R.R. U–pb dating of monazite and its application to geological problems. *Can. J. Earth Sci.* **1990**, *27*, 1431–1450. [CrossRef]
5. Tobgay, T.; McQuarrie, N.; Long, S.; Kohn, M.J.; Corrie, S.L. The age and rate of displacement along the main central thrust in the western bhutan himalaya. *Earth Planet. Sci. Lett.* **2012**, *319–320*, 146–158. [CrossRef]
6. Wawrzenitz, N.; Krohe, A.; Rhede, D.; Romer, R.L. Dating rock deformation with monazite: The impact of dissolution precipitation creep. *Lithos* **2012**, *134–135*, 52–74. [CrossRef]

7. Iizuka, T.; McCulloch, M.T.; Komiya, T.; Shibuya, T.; Ohta, K.; Ozawa, H.; Sugimura, E.; Collerson, K.D. Monazite geochronology and geochemistry of meta-sediments in the narryer gneiss complex, western australia: Constraints on the tectonothermal history and provenance. *Contrib. Mineral. Petrol.* **2010**, *160*, 803–823. [CrossRef]
8. Buick, I.S.; Clark, C.; Rubatto, D.; Hermann, J.; Pandit, M.; Hand, M. Constraints on the proterozoic evolution of the aravalli–delhi orogenic belt (nw india) from monazite geochronology and mineral trace element geochemistry. *Lithos* **2010**, *120*, 511–528. [CrossRef]
9. Corrie, S.L.; Kohn, M.J. Trace-element distributions in silicates during prograde metamorphic reactions: Implications for monazite formation. *J. Metamorph. Geol.* **2008**, *26*, 451–464. [CrossRef]
10. Kohn, M.J.; Vervoort, J.D. U-th-pb dating of monazite by single-collector icp-ms: Pitfalls and potential. *Geochem. Geophys. Geosyst.* **2008**, *9*. [CrossRef]
11. Schaltegger, U.; Schmitt, A.K.; Horstwood, M.S.A. U–th–pb zircon geochronology by id-tims, sims, and laser ablation icp-ms: Recipes, interpretations, and opportunities. *Chem. Geol.* **2015**, *402*, 89–110. [CrossRef]
12. Corrie, S.L.; Kohn, M.J. Resolving the timing of orogenesis in the western blue ridge, southern appalachians, via in situ id-tims monazite geochronology. *Geology* **2007**, *35*, 627. [CrossRef]
13. Košler, J.; Sláma, J.; Belousova, E.; Corfu, F.; Gehrels, G.E.; Gerdes, A.; Horstwood, M.S.A.; Sircombe, K.N.; Sylvester, P.J.; Tiepolo, M.; et al. U-pb detrital zircon analysis—Results of an inter-laboratory comparison. *Geostand. Geoanal. Res.* **2013**, *37*, 243–259. [CrossRef]
14. Fletcher, I.R.; McNaughton, N.J.; Davis, W.J.; Rasmussen, B. Matrix effects and calibration limitations in ion probe u–pb and th–pb dating of monazite. *Chem. Geol.* **2010**, *270*, 31–44. [CrossRef]
15. Peterman, E.M.; Hacker, B.R.; Grove, M.; Gehrels, G.E.; Mattinson, J.M. *A Multi-Method Approach to Improve Monazite Geochronology: TIMS, LA-ICP-MS, SIMS and EPMA*; American Geophysical Union: Washington, DC, USA, 2006.
16. Paquette, J.L.; Tiepolo, M. High resolution (5 µm) u–th–pb isotope dating of monazite with excimer laser ablation (ela)-icpms. *Chem. Geol.* **2007**, *240*, 222–237. [CrossRef]
17. Košler, J.; Tubrett, M.N.; Sylvester, P.J. Application of laser ablation icp-ms to u-th-pb dating of monazite. *Geostand. Geoanal. Res.* **2001**, *25*, 375–386. [CrossRef]
18. Horstwood, M.S.A.; Foster, G.L.; Parrish, R.R.; Noble, S.R.; Nowell, G.M. Common-pb corrected in situ u? Pb accessory mineral geochronology by la-mc-icp-ms. *J. Anal. At. Spectrom.* **2003**, *18*, 837. [CrossRef]
19. Aleinikoff, J.N.; Schenck, W.S.; Plank, M.O.; Srogi, L.; Fanning, C.M.; Kamo, S.L.; Bosbyshell, H. Deciphering igneous and metamorphic events in high-grade rocks of the wilmington complex, delaware: Morphology, cathodoluminescence and backscattered electron zoning, and shrimp u-pb geochronology of zircon and monazite. *Geol. Soc. Am. Bull.* **2006**, *118*, 39–64. [CrossRef]
20. Seydoux-Guillaume, A.-M.; Paquette, J.-L.; Wiedenbeck, M.; Montel, J.-M.; Heinrich, W. Experimental resetting of the u-th-pb systems in monazite. *Chem. Geol.* **2002**, *191*, 165–181. [CrossRef]
21. Palin, R.M.; Searle, M.P.; Waters, D.J.; Parrish, R.R.; Roberts, N.M.W.; Horstwood, M.S.A.; Yeh, M.W.; Chung, S.L.; Anh, T.T. A geochronological and petrological study of anatectic paragneiss and associated granite dykes from the day nui con voi metamorphic core complex, north vietnam: Constraints on the timing of metamorphism within the red river shear zone. *J. Metamorph. Geol.* **2013**, *31*, 359–387. [CrossRef]
22. Payne, J.L.; Hand, M.; Barovich, K.M.; Wade, B.P. Temporal constraints on the timing of high-grade metamorphism in the northern gawler craton: Implications for assembly of the australian proterozoic. *Aust. J. Earth Sci.* **2008**, *55*, 623–640. [CrossRef]
23. Williams, I.S.; Buick, I.S.; Cartwright, I. An extended episode of early mesoproterozoic metamorphic flow in the reynoldsrange, central australia. *J. Metamorph. Geol.* **1996**, *14*, 29–47. [CrossRef]
24. Didier, A.; Putlitz, B.; Baumgartner, L.P.; Bouvier, A.-S.; Vennemann, T.W. Evaluation of potential monazite reference materials for oxygen isotope analyses by sims and laser assisted fluorination. *Chem. Geol.* **2017**, *450*, 199–209. [CrossRef]
25. Burger, A.J.; von Knorring, O.; Clifford, T.N. Mineralogical and radiometric studies of monazite and sphene occurrences in the namib desert, south-west africa. *Mineral. Mag. J. Mineral. Soc.* **1965**, *35*, 519–528. [CrossRef]
26. Payne, J.L. Palaeo- to Mesoproterozoic Evolution of the Gawler Craton, Australia: Geochronological, Geochemical and Isotopic constraints. Ph.D. Thesis, University of Adelaide, Adelaide, Australia, 2008.

27. Gonçalves, G.O.; Lana, C.; Scholz, R.; Buick, I.S.; Gerdes, A.; Kamo, S.L.; Corfu, F.; Rubatto, D.; Wiedenbeck, M.; Nalini, H.A., Jr.; et al. The diamantina monazite: A new low-th reference material for microanalysis. *Geostand. Geoanal. Res.* **2018**, *42*, 25–47. [CrossRef]
28. Tomascak, P.B.; Krogstad, E.J.; Walker, R.J. U-pb monazite geochronology of granitic rocks from maine: Implications for late paleozoic tectonics in the northern appalachians. *J. Geol.* **1996**, *104*, 185–195. [CrossRef]
29. Alagna, K.E.; Petrelli, M.; Perugini, D.; Poli, G. Micro-analytical zircon and monazite u-pb isotope dating by laser ablation-inductively coupled plasma-quadrupole mass spectrometry. *Geostand. Geoanal. Res.* **2008**, *32*, 103–120. [CrossRef]
30. Peterman, E.M. Monazite standard assessment by la-icp-ms. *Geol. Soc. Am. Abstr. Programs* **2005**, *37*, 448.
31. Gasquet, D.; Bertrand, J.-M.; Pquette, J.-L.; Lehmann, J.; Ratzov, G.; De Ascencao Guedes, R.; Tiepolo, M.; Boullier, A.-M.; Scaillet, S.; Nomade, S. Miocene to messinian deformation and hydrothermal activity in a pre-alpine basement massif of the french western alps: New u-th-pb and argon ages from the lauzière massif. *Bull. Soc. Géol. Fr.* **2010**, *181*, 227–241. [CrossRef]
32. Liu, Z.-C.; Wu, F.-Y.; Yang, Y.-H.; Yang, J.-H.; Wilde, S.A. Neodymium isotopic compositions of the standard monazites used in uthpb geochronology. *Chem. Geol.* **2012**, *334*, 221–239. [CrossRef]
33. Tollo, R.P.; Aleinikoff, J.N.; Borduas, E.A.; Dickin, A.P.; McNutt, R.H.; Fanning, C.M. Grenvillian magmatism in the northern virginia blue ridge: Petrologic implications of episodic granitic magma production and the significance of postorogenic a-type charnockite. *Precambrian Res.* **2006**, *151*, 224–264. [CrossRef]
34. Gerbi, C.; West, D.P., Jr. Use of u/pb geochronology to identify successive, spatially overlapping tectonic episodes during silurian–devonian orogenesis in south-central maine, USA. *Geol. Soc. Am. Bull.* **2007**, *119*, 1218–1231. [CrossRef]
35. Pullen, A.; Kapp, P.; Gehrels, G.E.; DeCelles, P.G.; Brwon, E.H.; Fabijanic, J.M.; Ding, L. Gangdese retroarc thrust belt and foreland basin deposits in the damxung area, southern tibet. *J. Asian Earth Sci.* **2008**, *33*, 323–336. [CrossRef]
36. Buick, I.S.; Lana, C.; Gregory, C. A la-icp-ms and shrimp u/pb age constraint on the timing of ree mineralisation associated with bushveld granites. *S. Afr. J. Geol.* **2011**, *114*, 1–14. [CrossRef]
37. Morrissey, L.; Payne, J.L.; Kelsey, D.E.; Hand, M. Grenvillian-aged reworking in the north australian craton, central australia: Constraints from geochronology and modelled phase equilibria. *Precambrian Res.* **2011**, *191*, 141–165. [CrossRef]
38. Anderson, J.R.; Payne, J.L.; Kelsey, D.E.; Hand, M.; Collins, A.S.; Santosh, M. High-pressure granulites at the dawn of the proterozoic. *Geology* **2012**, *40*, 431–434. [CrossRef]
39. Maidment, D.W.; Hand, M.; Williams, I.S. Tectonic cycles in the strangways metamorphic complex, arunta inlier, central australia: Geochronological evidence for exhumation and basin formation between two high-grade metamorphic events*. *Aust. J. Earth Sci.* **2005**, *52*, 205–215. [CrossRef]
40. Payne, J.L.; Barovich, K.M.; Hand, M. Provenance of metasedimentary rocks in the northern gawler craton, australia: Implications for palaeoproterozoic reconstructions. *Precambrian Res.* **2006**, *148*, 275–291. [CrossRef]
41. Hand, M.; Mawby, J.; Miller, J. U– pb ages from the harts range, central australia; evidence for early ordovician extension and constraints on carboniferous metamorphism. *J. Geol. Soc. Lond.* **1999**, *156*, 715–730. [CrossRef]
42. Maidment, D.W. Paleozoic High-Grade Metamorphism within Centralian Superbasin, Harts Range Region, Central Australia. Ph.D. Thesis, Australian National University, Canberra, Australia, 2005.
43. Cutts, K.; Hand, M.; Kelsey, D.E. Evidence for early mesoproterozoic (ca. 1590 ma) ultrahigh-temperature metamorphism in southern australia. *Lithos* **2011**, *124*, 1–16. [CrossRef]
44. Szupunar, M.; Wade, B.; Hand, M.P.; Barovich, K.M. Timing of proterozoic high-grade metamorphism in the barossa complex, southern south australia: Exploring the extent of the 1590 ma event. *MESA J.* **2007**, *47*, 21–27.
45. Howard, K.E.; Hand, M.; Barovich, K.M.; Payne, J.L.; Cutts, K.; Belousova, E. U-pb zircon, zircon hf and whole-rock sm-nd isotopic constraints on the evolution of paleoproterozoic rocks in the northern gawler craton. *Aust. J. Earth Sci.* **2011**, *58*, 615–638. [CrossRef]
46. Seydoux-Guillaume, A.-M.; Wirth, R.; Deutsch, A.; Schärer, U. Microstructure of 24-1928 ma concordant monazites; implications for geochronology and nuclear waste deposits. *Geochim. Cosmochim. Acta* **2004**, *68*, 2517–2527. [CrossRef]

47. Cruz, M.J.; Cunha, J.C.; Merlet, C.; Sabate, P. Datacao pontual das monazitas da regiao de itambé, bahia, através da microssonda electronica. In *XXXIX Congresso Brasileiro de Geologia*; Sociedade Brasileira de Geologià–Núcleo Bahià: Salvador, Brazil, 1996; pp. 206–209.
48. Gonçalves, G.O.; Lana, C.; Scholz, R.; Buick, I.S.; Gerdes, A.; Kamo, S.L.; Corfu, F.; Marinho, M.M.; Chaves, A.O.; Valeriano, C.; et al. An assessment of monazite from the itambé pegmatite district for use as u–pb isotope reference material for microanalysis and implications for the origin of the "moacyr" monazite. *Chem. Geol.* **2016**, *424*, 30–50. [CrossRef]
49. Bleeker, W. Evolution of the Thompson Nickel Belt and Its Nickel Deposits, Manitoba, Canada. Ph.D. Thesis, University of New Brunswick, Fredericton, NB, Canada, 1990.
50. Burnham, O.M.; Halden, N.; Layton-Matthews, D.; Lesher, C.M.; Liwanag, J.; Heaman, L.; Hulbert, L.; Machado, N.; Michalak, D.; Pacey, M.; et al. Camiro project 97e-02, thompson nickel belt: Final report march 2002, revised and updated 2003; manitoba science, technology, energy and mines. *Manit. Geol. Surv.* **2009**, 434.
51. Taylor, J. The Anatectic History of Archean Metasediemntary Granulites from the Ancient Gneiss Complex, Swaziland. Ph.D. Thesis, University of Stellenbosch, Stellenbosch, South Africa, 2012.
52. Groppo, C.; Rubatto, D.; Rolfo, F.; Lombardo, B. Early oligocene partial melting in the main central thrust zone (arun valley, eastern nepal himalaya). *Lithos* **2010**, *118*, 287–301. [CrossRef]
53. Rutland, R.R.; Williams, I.S.; Korsman, K. Pre-1.91 ga deformation and metamorphism in the palaeo-proterozoic vammla migmatite belt, southern finland, and implications for svecofennian tectonics. *Bull. Geol. Soc. Finl.* **2004**, *76*, 93–140. [CrossRef]
54. Williams, I.S. Response of detrital zircon and monazite, and their u-pb isotopic systems, to regional metamorphism and host-rock partial melting, cooma complex, southeastern australia. *Aust. J. Earth Sci.* **2001**, *48*, 557–580. [CrossRef]
55. Seydoux-Guillaume, A.M.; Wirth, R.; Nasdala, L.; Gottschalk, M.; Montel, J.M.; Heinrich, W. An xrd, tem and raman study of experimentally annealed natural monazite. *Phys. Chem. Miner.* **2002**, *29*, 240–253. [CrossRef]
56. Simonetti, A.; Heaman, L.M.; Chacko, T.; Banerjee, N.R. In situ petrographic thin section u–pb dating of zircon, monazite, and titanite using laser ablation–mc–icp-ms. *Int. J. Mass Spectrom.* **2006**, *253*, 87–97. [CrossRef]
57. Paton, C.; Hellstrom, J.; Paul, B.; Woodhead, J.; Hergt, J. Iolite: Freeware for the visualisation and processing of mass spectrometric data. *J. Anal. At. Spectrom.* **2011**, *26*, 2508–2518. [CrossRef]
58. Paton, C.; Woodhead, J.D.; Hellstrom, J.C.; Hergt, J.M.; Greig, A.; Maas, R. Improved laser ablation u-pb zircon geochronology through robust downhole fractionation correction. *Geochem. Geophys. Geosyst.* **2010**, *11*. [CrossRef]
59. Steiger, R.H.; Jäger, E. Subcommission on geochronology: Convention on the use of decay constants in geo- and cosmochronology. *Earth Planet. Sci. Lett.* **1977**, *36*, 359–362. [CrossRef]
60. Hiess, J.; Condon, D.J.; McLean, N.; Noble, S.R. 238u/235u systematics in terrestrial uranium-bearing minerals. *Science* **2012**, *335*, 1610–1614. [CrossRef] [PubMed]
61. Eggins, S.M.; Kinsley, L.P.J.; Shelly, J.M.G. Deposition and element fractionation process during atmospheric pressure laser sampling for analysis by icp-ms. *Appl. Surf. Sci.* **1998**, *127–129*, 278–286. [CrossRef]
62. Jackson, S.E.; Pearson, N.J.; Griffin, W.L.; Belousova, E.A. The application of laser ablation-inductively coupled plasma-mass spectrometry to in situ u–pb zircon geochronology. *Chem. Geol.* **2004**, *211*, 47–69. [CrossRef]
63. Zack, T.; Stockli, D.F.; Luvizotto, G.L.; Barth, M.G.; Belousova, E.; Wolfe, M.R.; Hinton, R.W. In situ u–pb rutile dating by la-icp-ms: 208pb correction and prospects for geological applications. *Contrib. Mineral. Petrol.* **2011**, *162*, 515–530. [CrossRef]
64. Ludwig, K.R. *Isoplot/ex: A Geochronological Toolkit for Microsoft Excel*; Berkeley Geochronology Center: Berkeley, CA, USA, 2012; p. 53.
65. McFarlane, C.; Luo, Y. Modern analytical facilities. *Geosci. Can.* **2012**, *39*, 158–172.
66. Guillong, M.; Heinrich, C.A. Sensitivity enhancement in laser ablation icp-ms using small amounts of hydrogen in the carrier gas. *J. Anal. At. Spectrom.* **2007**, *22*, 1488–1494. [CrossRef]
67. Crowley, J.L.; Ghent, E.D. An electron microprobe study of the u–th–pb systematics of metamorphosed monazite: The role of pb diffusion versus overgrowth and recrystallization. *Chem. Geol.* **1999**, *157*, 285–302. [CrossRef]

68. Harlov, D.E.; Förster, H.J.; Nijland, T.G. Fluid-induced nucleation of (y+ree)-phosphate minerals within apatite: Nature and experiment. Part i. Chlorapatite. *Am. Mineral.* **2002**, *87*, 245–261. [CrossRef]
69. Williams, M.L.; Jercinovic, M.J.; Harlov, D.E.; Budzyn, B.; Hetherington, C.J. Resetting monazite ages during fluid-related alteration. *Chem. Geol.* **2011**, *283*, 218–225. [CrossRef]
70. Pyle, J.M.; Spear, F.S.; Rudnick, R.L.; MCDonough, W.F. Monazite-xenotime-garnet equilibrium in metapelites and a new monazite-garnet thermometer. *J. Petrol.* **2001**, *42*, 2083–2107. [CrossRef]
71. Klötzli, U.; Klötzli, E.; Günes, Z.; Kosler, J. Accuracy of laser ablation u-pb zircon dating: Results from a test using five different reference zircon. *Geostand. Geoanal. Res.* **2009**, *33*, 5–15. [CrossRef]